Universitat de Girona
Escola Politècnica Superior

Treball Final de Màster

Estudi: Màster en Ciència de Dades

Títol: Plataforma per Classificar Melanomes

Document: Memòria

Alumne: Wilber Eduardo Bermeo Quito

Tutor: Rafael Garcia Campos
Departament: ARQUITECTURA I TECNOLOGIA DE COMPUTADORS
Àrea: ARQUITECTURA I TECNOLOGIA DE COMPUTADORS

Convocatòria (mes/any): Setembre 2023

Universitat de Girona
Escola Politècnica Superior

MASTER'S THESIS

A Platform for Classifying Melanoma

WILBER EDUARDO BERMEO QUITO
September 2023

Master in Data Science

Advisors:

DR. RAFAEL GARCIA CAMPOS
University of Girona
Departament of Computer Architecture and Technology

SR. LUIS PLA LLOPIS
Accenture S.L.

Abstract

We present a platform for Melanoma Classification, leveraging a technical infrastructure based on Convolution Neural Network (CNN) models based on ResNet18.

For training and validation, exclusively we have utilized image data, and no additional metadata is incorporated during the training process. Various training strategies, such as data augmentation, learning rate decay, dropout, etc., were employed to enhance models performance.

The resulting models are accessible through a API, enabling users to interact with them via a straightforward web application. Users can submit batches of images to the API for classification, contributing to a user-friendly experience.

This platform demonstrates the efficacy of CNNs in melanoma classification, highlighting the importance of diverse training approaches. The API provides a practical interface for users to seamlessly integrate melanoma classification into their workflows.

1 Introduction

Skin cancer, including melanoma, is a significant global public health concern. Melanoma presents a considerable challenge due to its high mortality rate and the critical importance of early detection for successful treatment. Cancer begins when healthy cells undergo changes that cause them to grow and divide uncontrollably, forming tumors. These tumors can be classified as either cancerous (malignant) or non-cancerous (benign).

In recent times, there has been a growing focus on automating tasks in the medical field through Computer-Aided Diagnosis (CAD)[1]. Some studies have demonstrated that these systems can achieve results similar to those of professionals. However, the integration of CAD into the medical system remains a significant challenge.

The development of a CAD system necessitates the creation of models capable of effectively classifying melanoma. The SIIM-ISIC Melanoma Classification challenge specifically tasks participants with building models for identifying melanoma using skin lesion images and associated metadata. This thesis outlines our approach, wherein we leverage data from this challenge to train our models and subsequently expose them through our platform. By doing so, we contribute to the ongoing efforts to bridge the gap between cutting-edge medical imaging technology and practical clinical applications.

[1] CAD refers to the use of computer algorithms and technologies to assist healthcare professionals in the process of medical diagnosis.

2 Objectives

The final objective of this thesis is to craft a CAD infrastructure, focused on melanoma detection using deep learning vision models capable of detecting melanoma on dermoscopy images. To this end, the gradual achievements that must be accomplished are:

- Gaining a comprehensive understanding of the theory behind deep learning vision models and its practical applications.
- Select a base transfer model. Is the model good enough?, the selection of this model is given by the technical limitations?, or any other justification.
- Study different approaches to train the models and select a good evaluate metric given the dataset distribution of dermoscopy images.
- Develop the CAD infrastructure. It should contain the trained models, a simple web UI[2], an API[3] and finally a mechanism using Docker to create the images of these services making it ease to deploy in any system that supports virtualization.

3 Development process

The project methodology employed in this endeavor follows a continuous process. The project incorporates the concept of utilizing idle time effectively. For instance, during the training of models, there are periods of idle time, which we exploited by concurrently working on other tasks related to developing the entire infrastructure. This approach allows for maximizing productivity throughout the project, see Figure 1.

[2]User Interface. Is the point of human-computer interaction and communication in a device.

[3]Application Programming Interface. Is a set of protocols, routines, tools, and definitions that allow different software applications to communicate with each othe

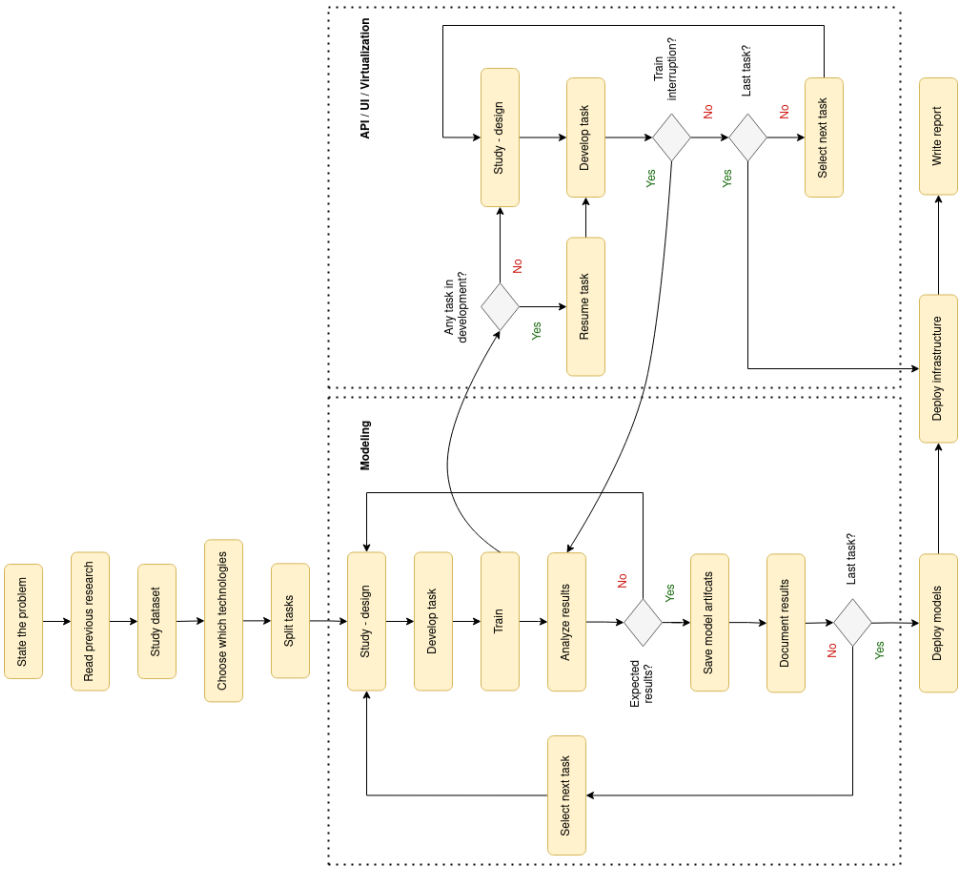

Figure 1: *Development process methodology.*

4 CAD infrastructure pipeline

Our CAD infrastructure pipeline (see Figure 2), consists of different steps, beginning with data acquisition, followed by data preprocessing. We then set up different datasets for training, validation, and testing. Subsequently, we train the models and, assess the models gathering metrics and finally we deploy the models under an API.

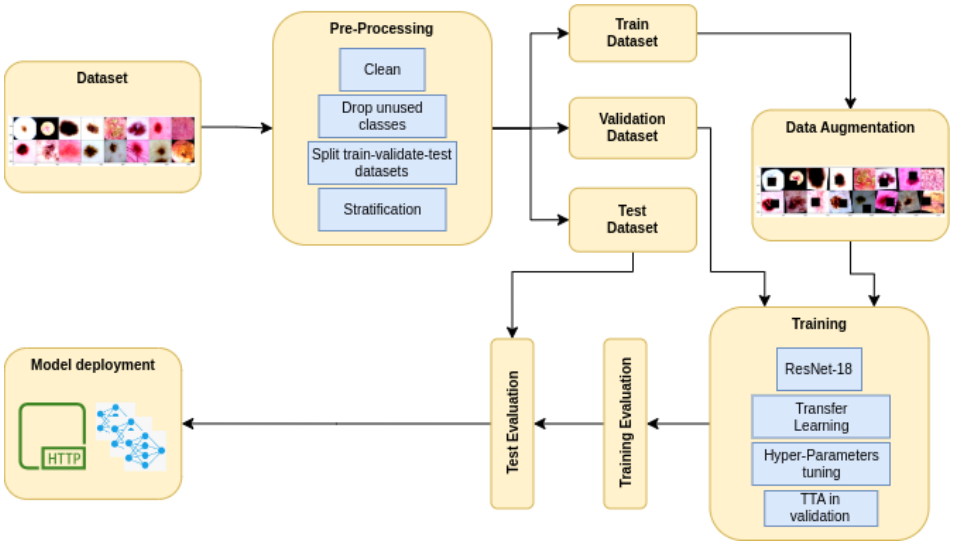

Figure 2: *CAD infrastructure pipeline. Train, test and deploy.*

5 Data and training strategies

Inspired by the approach of the Winning Solution to the SIIM-ISIC Melanoma Classification Challenge [Q. Ha 2020]. The Winning Solution team observed that in the entire dataset of 2020, comprising 33K images, only 1.76% were positive samples (i.e., malignant). In response, they decided to augment this data by incorporating information from the datasets of the same competition from the previous years (2018 and 2019). Although the individual datasets from these earlier years were smaller, totaling 25K images, they exhibited a positive ratio of 17.85%. This strategic combination allowed for a more balanced representation of positive cases in the training data.

To build the original dataset, we utilized eight classes selected from the raw dataset, as the remaining classes we considered not significant or there were very few samples of them. Any sample that was not categorized as one of the following classes were excluded from the training process.

- melanoma
- nevus
- BCC (Basal Cell Carcinoma)
- BKL (Benign lesions of the keratosis)
- AK (Actinic Keratosis)
- SCC (Squamous Cell Carcinoma)
- VASC (Vascular Lesions)
- DF (Dermatofibroma)

The filtered dataset comprises 31,265 distinct image samples, demonstrating a highly imbalanced dataset, as evident from Figure 3.

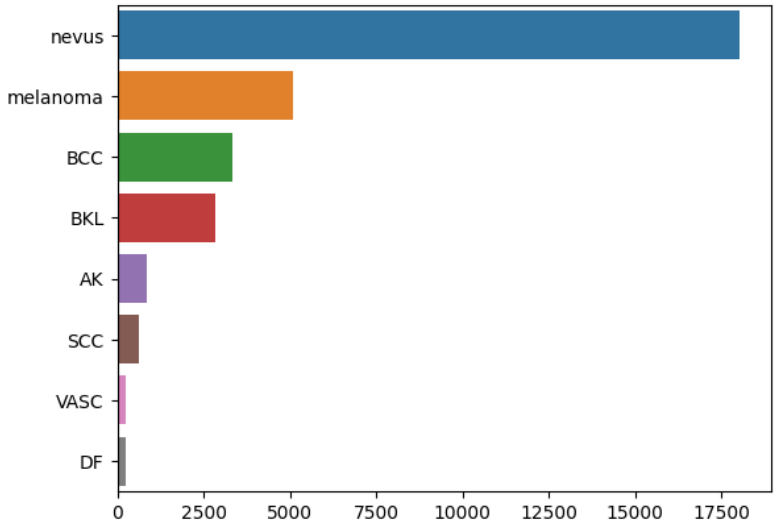

Figure 3: *Categories distribution in dataset.*

We started dividing the original dataset into three subsets using the Holdout set scheme, see Figure 4.

During the training phase, the test set remains completely separate and is not used in any way to configure the hyper-parameters. This ensures that the performance of a model on the test set is not artificially inflated by adjusting hyper-parameters to achieve an exceptionally good outcome in the validation set.

The data from the ISIC Archive was divided using the following percentages: 80% for training, 10% for validation, and 10% for testing. Each subset contain the same distribution of classes as the original dataset, i.e., we applied stratification.

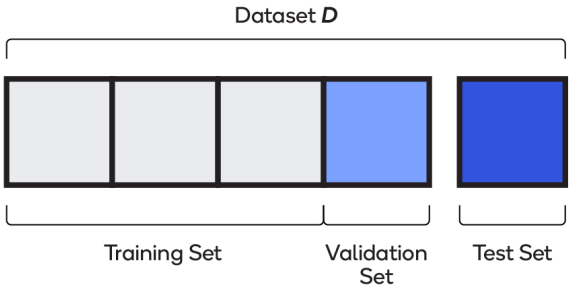

Figure 4: *Holdout set scheme. Illustration by Qualcomm*

In small to medium sized datasets, augmentation is important to prevent overfit. For some of our trained models, we used in the training dataset our augmentation pipelines, as illustrated in Figure 5 and Figure 6, with contains the following augmentations from the popular and powerful PyTorch augmentation library Albumentations [uslaev 2020]: Transpose, Flip, Rotate, RandomBrightness, RandomContrast, MotionBlur, MedianBlur, Gaus- sianBlur, GaussNoise, OpticalDistortion, GridDistortion, ElasticTransform, CLAHE, HueSaturationValue, ShiftScaleRotate, Cutout.

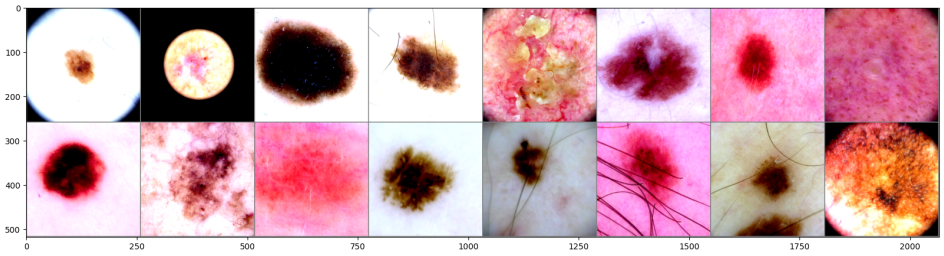

Figure 5: *Random sample of images.*

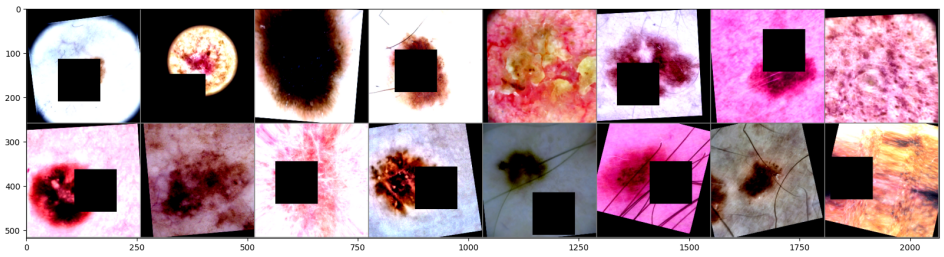

Figure 6: *Augmented random sample of images.*

We decided to use as transfer model an already trained ResNet in the ImageNet database. ResNet is short for "Residual Network," is a deep convolutional neural network (CNN) architecture that was introduced in 2015 by researchers from Microsoft Research [Kaiming He 2013]. It revolutionized the field of deep learning by addressing the challenge of training very deep neural networks.

There are various architectural variants or "flavors" of ResNet, including ResNet-152, ResNet-101, ResNet-50, ResNet-34, and ResNet-18. The number following the name of each ResNet variant indicates the number of inner layers present in the architecture. The more the number of the layers the more the accuracy, yet the number of parameters to be trained increase. To accurately assess the performance of each ResNet architecture, refer to Table 1, which provides the accuracy achieved on the ImageNet dataset along with the corresponding number of trainable parameters in millions.

Model	Accuracy	Parameters
ResNet-152	78.31%	60.2M
ResNet-101	77.37%	44.5M
ResNet-50	76.15%	25.6M
ResNet-34	73.30%	21.8M
ResNet-18	69.76%	11.7M

Table 1: *Accuracy achieved on ImageNet and trainable parameters of each ResNet. Each image in the ImageNet dataset is associated with 1 of 1,000 classes. Table by paperswithcode*

We decided to use ResNet18 as base model only for technical reasons and time constrains. The lack of powerfull GPUs took us to pick this estimator agains the others. There are other architectures that we could have tried as: AlexNet, ResNetXt, VGG, etc, but comparing the performance of those models in the SIIM-ISIC Melanoma competition is not the goal of this thesis.

Upon the ResNet18 we propose two models. For both models, we transformed their last layer into an identity layer, i.e., $\mathbf{y} = Identity(\mathbf{y}), \quad \mathbf{y} \in \mathbb{R}^{512}$ and added a new trainable linear layer, $\mathbf{y} = Linear(\mathbf{x}), \quad \mathbf{y} \in \mathbb{R}^{8}, \quad \mathbf{x} \in \mathbb{R}^{512}$.

To train the models, we only need to define the forward propagation. The result of the forward propagation for the first model is given by:

$$\mathbf{y} = Forward(\mathbf{x}) = Linear(ResNet18(\mathbf{x})),$$

where $\mathbf{y} \in \mathbb{R}^8$, and $\mathbf{x} \in \mathbb{R}^{3\times256\times256}$. Figure 7 shows the architecture of the first model.

Layer (type:depth-idx)	Input Shape	Output Shape	Param #
ResNet18_Melanoma	[1, 3, 256, 256]	[1, 8]	--
├─ResNet: 1-1	[1, 3, 256, 256]	[1, 512]	--
│ └─Conv2d: 2-1	[1, 3, 256, 256]	[1, 64, 128, 128]	9,408
│ └─BatchNorm2d: 2-2	[1, 64, 128, 128]	[1, 64, 128, 128]	128
│ └─ReLU: 2-3	[1, 64, 128, 128]	[1, 64, 128, 128]	--
│ └─MaxPool2d: 2-4	[1, 64, 128, 128]	[1, 64, 64, 64]	--
│ └─Sequential: 2-5	[1, 64, 64, 64]	[1, 64, 64, 64]	147,968
│ └─Sequential: 2-6	[1, 64, 64, 64]	[1, 128, 32, 32]	525,568
│ └─Sequential: 2-7	[1, 128, 32, 32]	[1, 256, 16, 16]	2,099,712
│ └─Sequential: 2-8	[1, 256, 16, 16]	[1, 512, 8, 8]	8,393,728
│ └─AdaptiveAvgPool2d: 2-9	[1, 512, 8, 8]	[1, 512, 1, 1]	--
│ └─Identity: 2-10	[1, 512]	[1, 512]	--
├─Linear: 1-2	[1, 512]	[1, 8]	4,104

Figure 7: *ResNet18 Melanoma architecture.*

The forward propagation of the second model is more intricate, involving the averaging of predictions N times through the application of $Linear \circ Dropout$.

$$\mathbf{y} = Forward(\mathbf{x}) = \frac{\sum_{j=1}^{N} Linear(Dropout(\mathbf{r}))}{\mathbf{N}},$$

where $\mathbf{y} \in \mathbb{R}^8$, $\mathbf{x} \in \mathbb{R}^{3\times256\times256}$, and $\mathbf{r} = ResNet18(\mathbf{x}), \quad \mathbf{r} \in \mathbb{R}^{512}$. Figure 8 shows the architecture of the second model.

Layer (type:depth-idx)	Input Shape	Output Shape	Param #
ResNet18_Dropout_Melanoma	[1, 3, 256, 256]	[1, 8]	--
├─ResNet: 1-1	[1, 3, 256, 256]	[1, 512]	--
│ └─Conv2d: 2-1	[1, 3, 256, 256]	[1, 64, 128, 128]	9,408
│ └─BatchNorm2d: 2-2	[1, 64, 128, 128]	[1, 64, 128, 128]	128
│ └─ReLU: 2-3	[1, 64, 128, 128]	[1, 64, 128, 128]	--
│ └─MaxPool2d: 2-4	[1, 64, 128, 128]	[1, 64, 64, 64]	--
│ └─Sequential: 2-5	[1, 64, 64, 64]	[1, 64, 64, 64]	147,968
│ └─Sequential: 2-6	[1, 64, 64, 64]	[1, 128, 32, 32]	525,568
│ └─Sequential: 2-7	[1, 128, 32, 32]	[1, 256, 16, 16]	2,099,712
│ └─Sequential: 2-8	[1, 256, 16, 16]	[1, 512, 8, 8]	8,393,728
│ └─AdaptiveAvgPool2d: 2-9	[1, 512, 8, 8]	[1, 512, 1, 1]	--
│ └─Identity: 2-10	[1, 512]	[1, 512]	--
├─ModuleList: 1-10	--	--	--
│ └─Dropout: 2-11	[1, 512]	[1, 512]	--
├─Linear: 1-3	[1, 512]	[1, 8]	4,104
├─ModuleList: 1-10	--	--	--
│ └─Dropout: 2-12	[1, 512]	[1, 512]	--
├─Linear: 1-5	[1, 512]	[1, 8]	(recursive)
├─ModuleList: 1-10	--	--	--
│ └─Dropout: 2-13	[1, 512]	[1, 512]	--
├─Linear: 1-7	[1, 512]	[1, 8]	(recursive)
├─ModuleList: 1-10	--	--	--
│ └─Dropout: 2-14	[1, 512]	[1, 512]	--
├─Linear: 1-9	[1, 512]	[1, 8]	(recursive)
├─ModuleList: 1-10	--	--	--
│ └─Dropout: 2-15	[1, 512]	[1, 512]	--
├─Linear: 1-11	[1, 512]	[1, 8]	(recursive)

Figure 8: *ResNet18 Dropout Melanoma architecture.*

6 Validation strategy

In any machine learning project, it is critical to establish a reliable validation scheme to properly evaluate and compare models. This becomes particularly crucial when dealing with a small to medium-sized dataset or when the evaluation metric is unstable, as is the case with the dataset provided in the competition. There are various metrics commonly used to assess the quality of a model's predictions. We present a selection of metrics that we find relevant for evaluating our models.

A confusion matrix (see Figure 9) is a square matrix with dimensions `NxN`, where `N` represents the total number of classes being predicted.

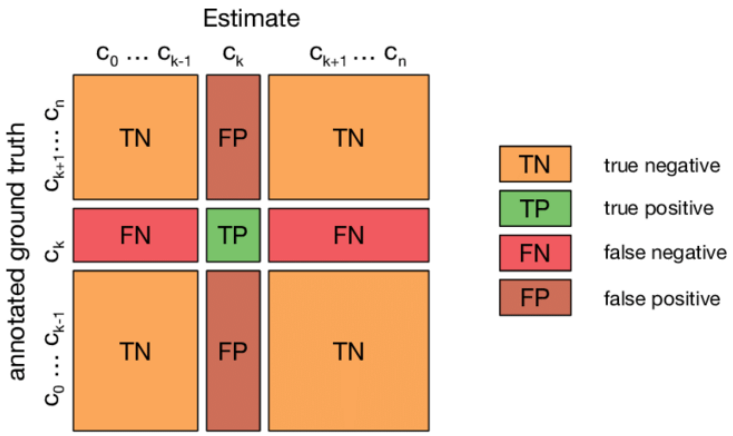

Figure 9: *Confusion matrix multi-class. Illustration by kaggle*

From confusion matrix we can obtain other metrics such as:

- **Accuracy**

  The Accuracy metric, calculates the ratio of correct predictions to the total number of predictions made on a dataset. It is not a good matric when working with unbalanced datasets.

$$Accuracy = \frac{TP + TN}{TP + TN + FP + FN}$$

- **True Positive Rate (TPR) or Sensitivity**

  The True Positive Rate tells about how many of the true class samples were correctly classified.

$$TPR = \frac{TP}{TP + FN}$$

- **False Positive Rate (FPR) or False Alarm Ratio**

  The False Positive Rate tells the proportion of the true class samples that were not correctly classified and are False Positive.

$$FPR = \frac{FP}{FP + TN}$$

- **Receiver Operator Characteristic (ROC)**

  An ROC curve plots TPR vs. FPR at different classification thresholds T, where T for $0 <= x <= 1$. Lowering the classification threshold classifies more items as positive, thus increasing both False Positives and True Positives. By plotting the curve, you can say which threshold is better, depeding on how many False Positive we are willing to accept.

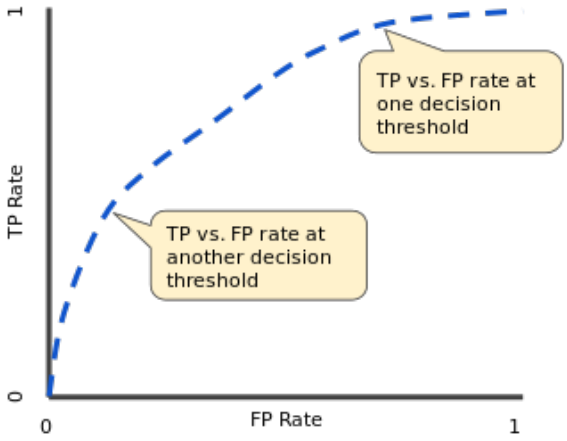

Figure 10: *Typical ROC Curve. Illustration by Alphabet Inc.*

- **Area Under the Curve (AUC)**

  The Area Under the Curve is a value between 0 and 1 that measures the ability of a classifier to distinguish between classes. It is used as a summary of the ROC curve. The higher the AUC, the better the performance of the model at distinguishing between the positive and negative classes.

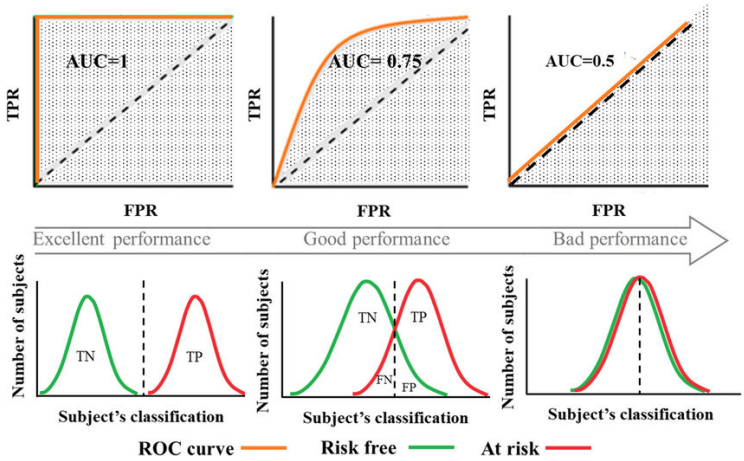

Figure 11: *AUC comparation. Illustration by Elizabeth Louise Thomas*

We used Test-time augmentation (TTA) in the inference phases, i.e., validation and testing. The idea behind TTA, is to generate multiple augmented versions of the test input and average the predictions of the model over these augmented samples to get a more robust and accurate result.

Let's denote the original test input as X and the model's prediction for X as Y. TTA involves generating N augmented versions per each X_i, obtaining predictions for each of these augmented samples $(Y_i^1, Y_i^2, ..., Y_i^N)$, and then averaging these predictions.

$$TTA(X_i) = \frac{1}{N}\sum_{j=1}^{N} f(j, Y_i^j)$$

Where:

- X is the original test input.
- Y is the model's prediction for the original input.
- X_i represents the i-th augmented version of the test input.
- Y_i is the model's prediction for the i-th augmented input.
- N is the number of augmented samples generated.
- f is defined as $f : Int \rightarrow X \rightarrow X$. The function applies simple transformations such as rotations and flips.

7 Model metrics

The training phase ended with the development of eight models. Various learning policies such as; Learning Decay with schedulers and regularization with Data Agumentation and Dropout were applied. We computed other metrics such as, recall and presition but in Table 3 we show the AUC metric of in all datasets for the all models.

The metrics with a gray background in Table 3 are from models that incorporated additional regularization techniques. These models were trained for 40 epochs since regularization tends to slow down the minimization of the objective function compared to the other models that were trained for only 20 epochs.

Models that used a scheduler during the training stage are denoted with a symbol next to their names. For reference, the mapping between the scheduler used and the corresponding symbol is provided in Table 2.

Scheduler Mapping	
$\star$	Step Learning Rate
$*$	Cosine Annealing Learning Rate
$\bullet$	Cosine Annealing Warm Restarts

Table 2: *Scheduler mapping.*

As a result, we conclude that the first group of models performed well on the test set with an average AUC of 88.875% and a small standard deviation of ±0.377%. However, they showed signs of overfitting in the training process, as model performed excelent in the training data but poorer in the validation set. In contrast, the second group of models that were trained with additional regularization techniques, achieved lower results in the test set, but did not suffer from overfitting. They had an average AUC of 84.950% with a standard deviation of ±0.625%.

8 CAD infrastructure result

In this section, we briefly present the CAD infrastructure in its entirety (see Figure 12). The CAD infrastructure essentially consists of two services: an API used to expose and interact with the trained models via the HTTP protocol, and a web application (UI). The UI features a simple layout that displays prediction data and metadata for dermoscopy images, along with information about the

	Train AUC	Val AUC	Test AUC
M0	0.952	0.903	0.892
M1 ⋆	0.947	0.900	0.892
M2 ∗	0.933	0.895	0.885
M3 •	0.935	0.896	0.886
M4	0.886	0.877	0.858
M5 ⋆	0.867	0.861	0.843
M6 ∗	0.874	0.868	0.848
M7 •	0.877	0.869	0.849
Mean	94.175%	89.850%	88.875%
SD	0.921%	0.370%	0.377%
Mean	87.600%	86.875%	84.950%
SD	0.787%	0.655%	0.625%

Table 3: *AUC metric in all datasets.*

model used for the prediction. For each service, we created a Docker image to facilitate easy deployment of the infrastructure on any system that supports virtualization.

The necessary steps to install the infrastructure are explained in the README of the repository where the research and source code are available. Please visit the repository at https://github.com/wilberquito/melanoma.thesis.

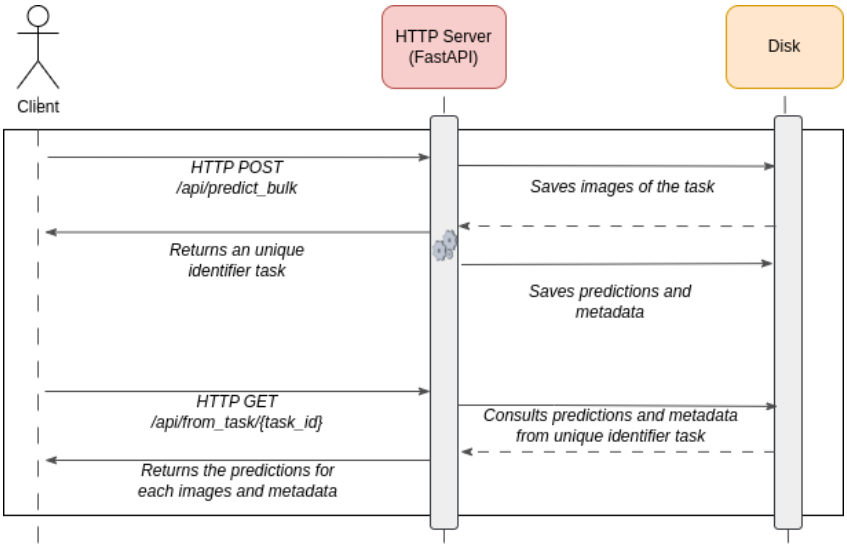

Figure 12: Comunication protocol for infering a bulk of dermoscopy images.

The API basically has 5 end-points.

- **Consult the exposed models**

  Request:

  ```
  http://<api>/public_models
  ```

  Possible response:

  ```
  {
    "models": [
      "M0",
      "M1",
      "M2",
      "M3",
      "M4",
      "M5",
      "M6",
      "M7",
      "vicorobot.8c_b3_768_512_18ep_best_20_fold0",
      "vicorobot.8c_b3_768_512_18ep_best_fold0",
      "vicorobot.8c_b3_768_512_18ep_final_fold0"
    ]
  }
  ```

- **Trigger inference for a simple image**

  This endpoint expects an HTTP request containing a JPEG image in the body, along with the specified model name for performing the inference.

  Request:

  ```
  POST http://<api>/predict?model_id=<model-id>
  ```

  Possible response:

  ```
  {
    "task_uuid": "721445f5-ff37-4c99-af74-7157925b4a7c"
  }
  ```

- **Trigger inference for a bulk of images**

  This endpoint is designed to handle requests for predicting multiple images simultaneously. To use this endpoint, you are required to provide two pieces of information in the HTTP request: the model you wish to use for image inference and a list of images attached to the request body.

  Request:

  ```
  http://<api>/predict_bulk?model_id=<model-id>
  ```

  Possible response:

```
{
  "task_uuid": "77d5e834-60a1-49b6-a71a-b3472dc21ce5",
  "num_images": 2
}
```


- **Consult the results of a triggered inference**

  Given the unique identifier for a triggered task inference, we can consult the result of the inference.

  Request:

  ```
  http://<api>/from_task/<task_uuid>
  ```

  Possbile response:


```
[
  {
    "name": "ISIC_0052349.jpg",
    "probabilities": {
      "AK": 0.0007466986,
      "BCC": 0.0005002805,
      "BKL": 0.015733117,
      "DF": 0.00086343783,
      "SCC": 0.0007902466,
      "VASC": 0.0017217622,
      "melanoma": 0.017426228,
      "nevus": 0.9622182
    },
    "metadata": {
      "origin": "wilberquito",
      "net_type": "resnet18",
      "img_size": 256,
      "out_dim": 8
    },
    "prediction": {
      "target": false,
      "label": 7,
      "prediction": "nevus"
    }
  },
  {
    "name": "ISIC_1766619.jpg",
    "probabilities": {
      "AK": 0.00016253705,
      "BCC": 0.00011373816,
      "BKL": 0.00052201655,
      "DF": 0.0006251502,
      "SCC": 0.00032183932,
      "VASC": 0.00025595966,
      "melanoma": 0.0012655357,
      "nevus": 0.9967333
    },
    "metadata": {
      "origin": "wilberquito",
      "net_type": "resnet18",
      "img_size": 256,
      "out_dim": 8
    },
```

```
    "prediction": {
      "target": false,
      "label": 7,
      "prediction": "nevus"
    }
  }
]
```

- **Consult the public end-points**

  All end-points are easy accessible by consulting the documentation.

  ```
  http://<api>/docs
  ```

Upon accessing the UI service through your web browser, you will immediately notice a single-page web application with several interactive buttons (see Figure 13).

Figure 13: *Main interactive buttons of the UI service.*

1. This button serves a dual purpose based on the UI's current state. Either allows user make the prediction request or reset the UI clearing the results of a inference.

2. This button enables users to load images directly from their device, see Figure 14 and Figure 15.

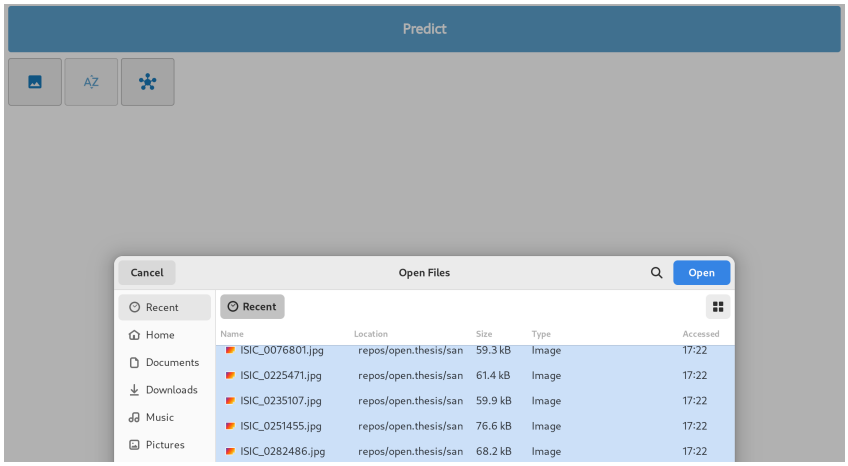

Figure 14: *Loading dermoscopy images from device.*

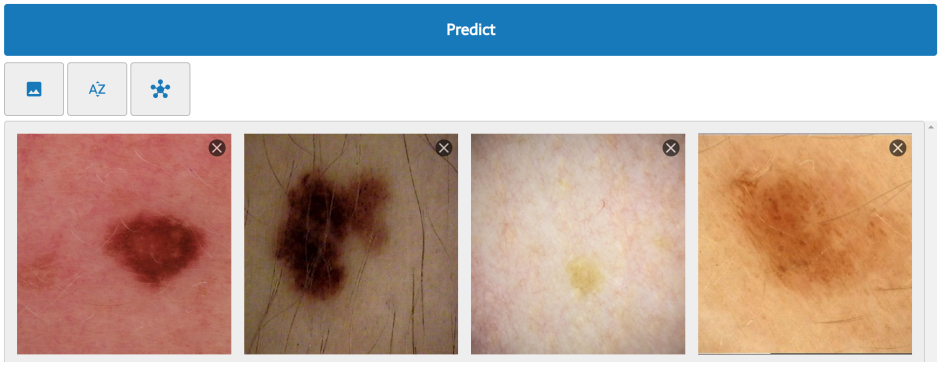

Figure 15: *Dermoscopy images loaded in the UI.*

3. Designed to sort the loaded images in the UI, this button operates differently depending on whether the inference has been performed. If the inference has not been executed, it sorts the images by name. However, if the inference results have been obtained from the API, the button sorts the images by importance, prioritizing melanoma classifications followed by others.

4. This button displays a list of models exposed by the API, see Figure 16.

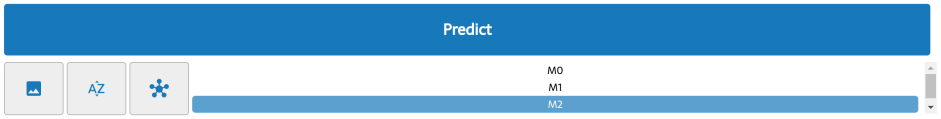

Figure 16: *Selecting exposed models by the API.*

Once we have loaded the images and selected the desired model for prediction, we are ready to make the request to the API for inference using the chosen model. The UI will display the images classified as melanoma with a red background and the images classified as other classes with a blue background, see Figure 17.

On the top-right corner of every image appears button with a square symbol. When you click on any of these buttons, a pop-up window appears, providing additional information about the prediction for that specific image.

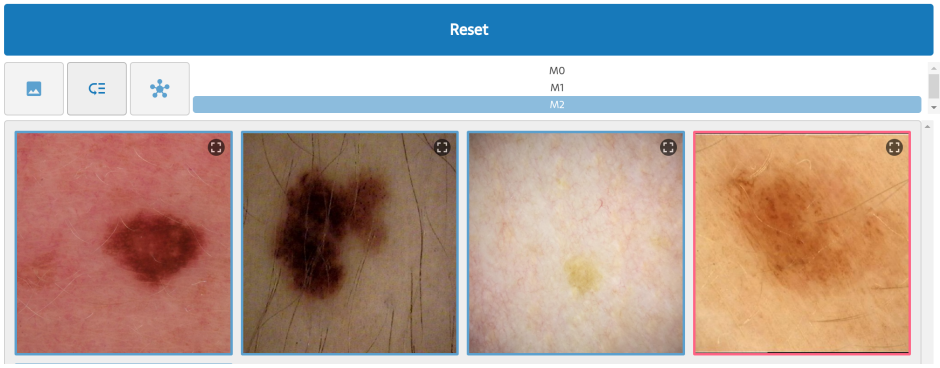

Figure 17: *UI state after prediction response.*

For instance, let's inquire about more information about the dermoscopy image that was classified as melanoma in Figure 17. Clicking on the corresponding square button will trigger a pop-up as showed in Figure 18. The pop-up provides extra information about the prediction, image, mode's author, etc.

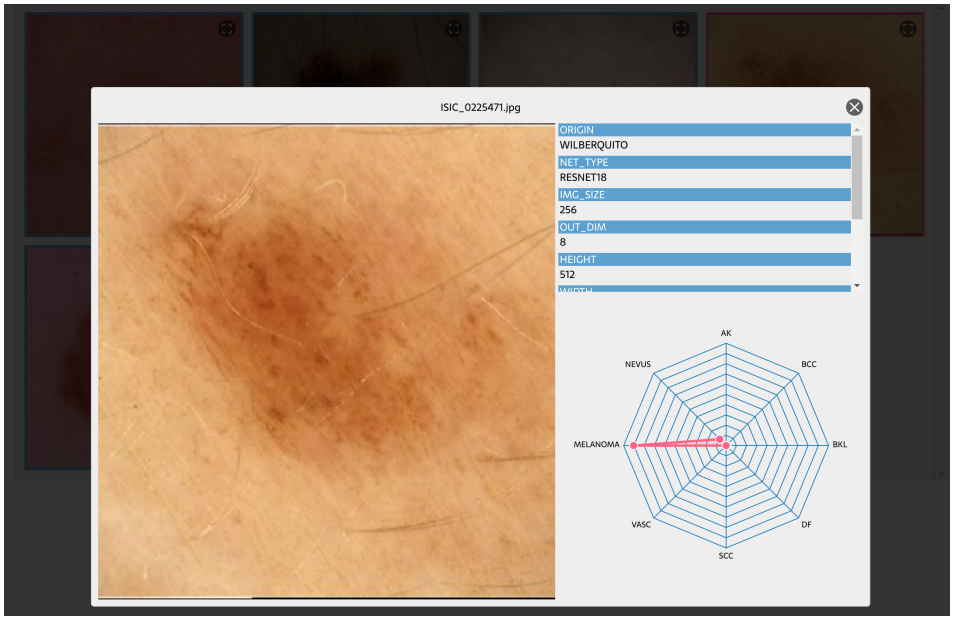

Figure 18: *Extra prediction information.*

9 Conclusions and Future Work

The main goal of this thesis was to utilize machine learning techniques to train multiple CNNs models for detecting melanoma in an imbalanced dataset of dermoscopy images, adding value creating a CAD infrastructure to make models

easy available to make predictions.

While the models were in the training phase, we took the opportunity to develop the CAD (Computer-Aided Diagnosis) infrastructure. For the API, we opted for a soft-configuration approach, where the configurations are specified through file-based configurations, providing flexibility and ease of management. Additionally, we designed a simple and intuitive user interface (UI) to streamline the interaction of healthcare professionals with the exposed models.

Furthermore, we achieved a significant milestone by successfully implementing a mechanism for deploying the models and services using containers. By leveraging containers, we ensured that the entire CAD architecture could be easily replicated and deployed across different environments. To further simplify the setup process, we also developed a shell script capable of downloading the necessary images and initiating the container services effectively.

This approach combined both research and engineering efforts, enabling us to make sophisticated knowledge accessible to a wider audience. By integrating cutting-edge research and engineering principles, we have created a powerful tool for medical professionals, providing them with advanced diagnostic capabilities to improve patient care and outcomes.

As we evaluate the current state of the CAD infrastructure, we acknowledge the existence of various potential implementations that could enhance its capabilities. One promising approach involves establishing a mechanism for iterative model training, continuously monitoring and tracking their performance. Models exhibiting exceptional behavior could be promptly exposed and made available for use. In the user interface (UI), professionals can access the training results of the models, even instances where the selected model may not have performed optimally. By providing this additional information, our aim is to boost professionals' confidence, preventing them from relying blindly on the models' inferences. Another promising approach involves exploring more complex CNN models or other architectures, such as the Transformer [Vaswani 2017].

The resulting CAD infrastructure is a tool to assist, not a replacement for human expertise in desition making.

Bibliography

[Kaiming He 2013] Xiangyu Zhang Kaiming He and Jian Sun. *Deep Residual Learning for Image Recognition*, 2013. Available at https://arxiv.org/pdf/1512.03385v1.pdf. (Cited on page 7.)

[Oncol 2021] W. Oncol. *Cutaneous Malignant Melanoma: A Review of Early Diagnosis and Management*, 2021. Available at https://www.ncbi.nlm.nih.gov/pmc/articles/PMC7935621/pdf/wjon-12-007.pdf. (Cited on page 21.)

[Q. Ha 2020] B. Liu Q. Ha and F. Liu. *Identifying Melanoma Images using EfficientNet Ensemble: Winning Solution to the SIIM-ISIC Melanoma Classification Challenge*, 2020. Available at https://arxiv.org/pdf/2010.05351.pdf. (Cited on page 4.)

[uslaev 2020] Eugene uslaev Alexande and Parinov. *Albumentations: Fast and Flexible Image Augmentations*, 2020. Available at https://www.mdpi.com/2078-2489/11/2/125. (Cited on page 6.)

[Vaswani 2017] Ashish. Vaswani. *Attention Is All You Need.*, 2017. Available at https://arxiv.org/abs/1706.03762. (Cited on page 20.)